OFFICE OF NAVAL RESEARCH

TECHNICAL REPORT

for

1 September 1989 through 28 February 1990

for

Contract N00014-89-J-3227

R&T No.

Fundamental Properties and Device Applications of Ge_xSi_{1-x}/Si Superlattices

Kang L. Wang

University of California, Los Angeles
405 Hilgard Avenue
Los Angeles, CA 90024

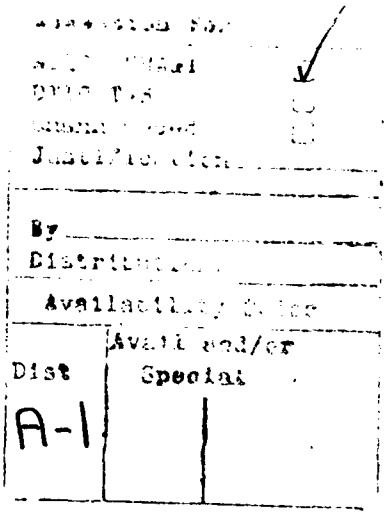

Contents

List of Figures

1 Abstract

The progress of the study of transport properties include the resonant tunneling and miniband transport in SiGe/Si heterostructures and a hot hole resonant tunneling transistor. Both light and heavy hole tunnelings were observed showing negative differential resistance. The tunneling species were identified by studying the magnetic field dependence of the tunneling peak positions. Our investigations have been extended for the study of miniband transport in SiGe/Si superlattices. In the area of quantum device, we have fabricated a hot hole resonant tunneling transistor. Preliminary results indicate that transistor action with controllable negative differential resistance can be achieved.

2 Introduction

In the following sections, we will describe the accomplishments made on device application of strained Ge_xSi_{1-x}/Si heterostructures. We have begun the investigation of quantum effects by fabricating resonant tunneling structures. Both light and heavy hole tunneling were observed in I(V), dI/dV characteristics. The tunneling species were identified by studying the magnetic field dependence of the tunneling peak positions. SiGe/Si superlattices were also been fabricated and the study of miniband transport was performed. The transport properties of minibands in SiGe/Si superlattices have been studied using both tunneling spectroscopy and thermionic emission. The activation energies estimated using thermionic analysis are in good agreement with the calculations using a transfer matrix technique including the light and heavy hole splitting. In the area of quantum devices, we have fabricated a hot hole resonant tunneling transistor. Preliminary results indicate that transistor action with controllable negative differential resistance can be achieved.

In the following we highlight the accomplishments made. Details may be referenced to the publications resulting from the research efforts under ONR support. These publications are cited in the descriptions.

3 Progress

3.1 Resonant Tunneling

Several double barrier resonant tunneling structures with various strain conditions have been grown by MBE [1]. The current-voltage I-V of the tunneling diode at 4.2 K, 77 K and 300 K are shown in Fig. 1. The negative differential resistance is clearly seen at 4.2 K and 77 K; however, at room temperature NDR is not visible. Inset of the Fig. 1 shows the I-V and conductance voltage (G-V) for an additional peak in the higher bias (> 500 mV). The experimental peak voltage positions are in agreement with the estimated values taking into account the bound-state energy and voltage drops across the spacer layers [1]. The peak at 300 mV has a peak-to-valley current ratio of 1.6 at 77 K. The predominant tunneling mechanism is confirmed to be due to the light hole. The latter is verified by investigating the tunneling under a strong magnetic field parallel to the interface. As the magnetic field is applied parallel to the interface, the motion of holes passing through the double barrier structure is detoured. This can be considered as a decrease of the kinetic energy in the tunneling direction or in other words, an effective increase of the tunneling barrier. In this case, the additional voltage needed for resonant tunneling through can be estimated [2] using WKB approximation to be about $eB^2(2s^2 + 2b^2 + w^2)/3m^*$, where s, b, and w are the thickness of the spacer, barrier and well, respectively. Figure 2 shows the magnetic field dependence of the voltage shift for the light and heavy hole peaks (solid lines) and from these dependencies, the light and heavy hole peaks can be clearly discriminated.

3.2 Superlattice Minibands

The successful demonstrations of resonant tunneling in the SiGe/Si heterostructures reveals the coherent nature of the carrier transport through the double barrier structure. This indicates that the study can be extended to structures involving multiple layers such as quantum wells and superlattices. Here, the results of the transport measurement of a symmetrically strained, $Si_{1-x}Ge_x/Si$ superlattice grown on a $Si_{1-x/2}Ge_{x/2}/Si$ buffer layer are presented. The superlattice structure is grown on a 2 μm thick unstrained p^+ $Si_{0.8}Ge_{0.2}$ buffer layer doped to 5×10^{18} cm^{-3}. The active

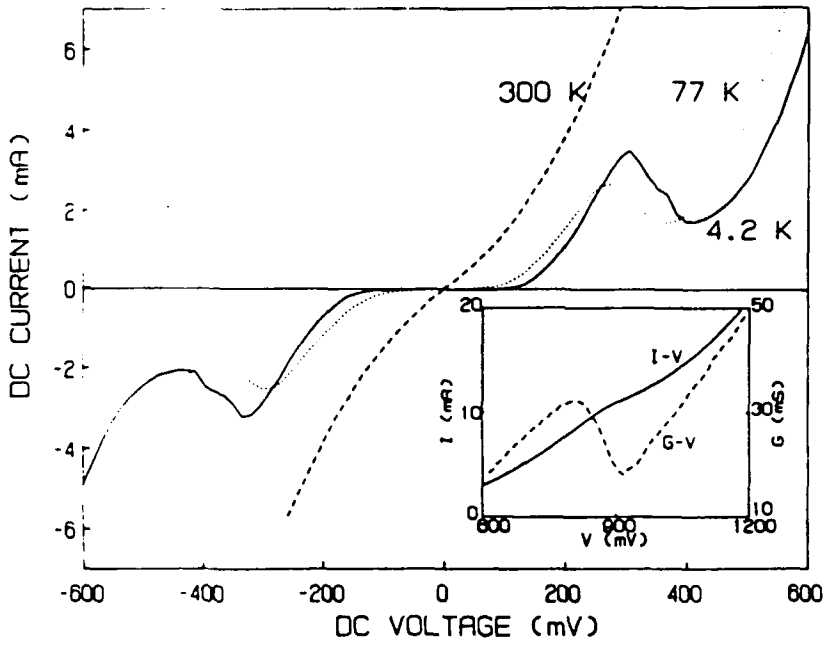

Figure 1: Observed I-V characteristics for the structure at 300 K, 77 K, and 4.2 K. Inset shows the I-V and conductance G-V measurement of an additional peak for high bias at 77 K.

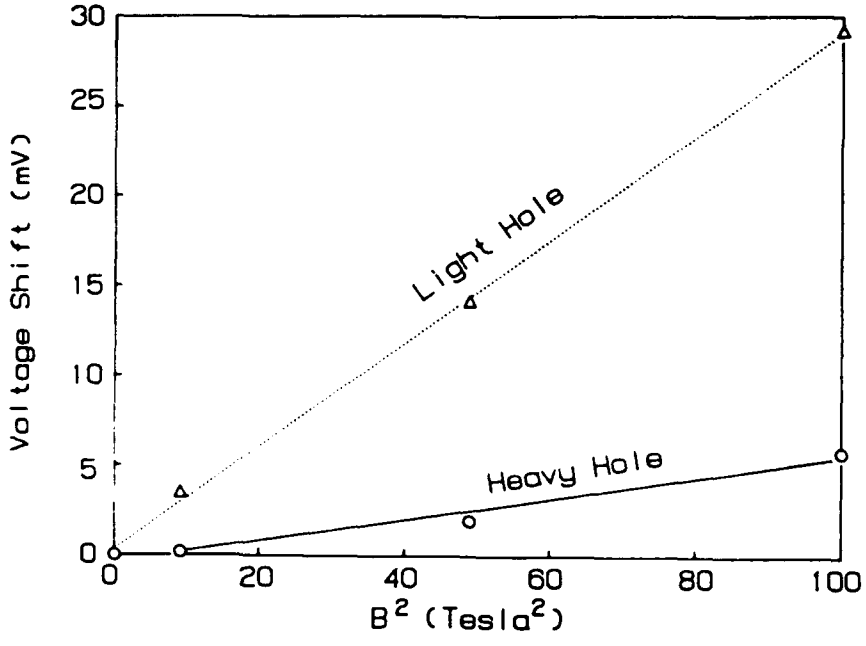

Figure 2: Measured peak voltage shift vs B^2 for the light hole (dotted line) and heavy hole (solid line) states when the magnetic field is parallel to the interfaces.

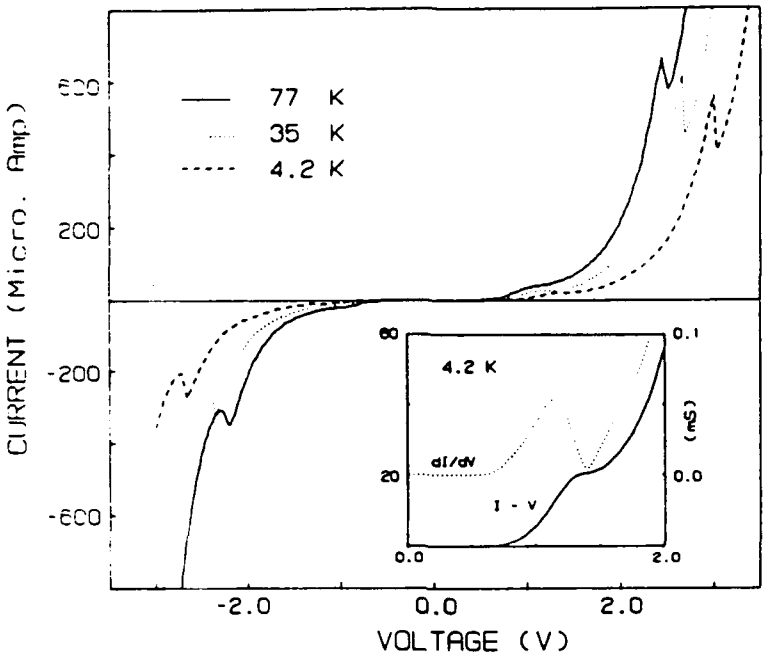

Figure 3: Observed current-voltage (I-V) at 77 K, 35 K and 4.2 K, showing conduction through minibands in the superlattice. Inset of the figure shows the magnified I-V, and dI(V)/dV for the first peak.

layers of the structure consist of a 15 period $Si_{0.6}Ge_{0.4}/Si$ (each layer 50 Å -thick) superlattice of p-doped (1×10^{17} cm^{-3}) and 150 Å undoped contact layers on each side of the superlattice.

Fig. 3 shows the measured I-V, and dI/dV at 4.2 K, 35 K and 77 K. Two peaks at 1.1 V and 2.5 V (77 K) are present in the I-V and dI/dV. The peak at 2.5 V shows a clear negative differential resistance. As the temperature of the sample decreases, the peak-to-valley ratio of the peak at 2.5 V increases, and the peak position shifts towards a higher voltage while the peak at 1.1 V becomes more apparent from the dI/dV curve. Above 100 K, the NDR is no longer clearly observed. The observed process is a result of miniband transport. When the Fermi level in the emitter region is aligned with one of the minibands the carriers flow through the miniband. The NDR shows up when the Fermi level is moved away from the miniband. Although the NDR due to conduction through the second miniband is clearly observed as shown in Fig. 3, no NDR is seen for the transport through the first miniband, probably due to its narrow bandwidth.

The energies of the minibands are also investigated experimentally using the I-V-T measurement. The experimental values for the first and second miniband positions

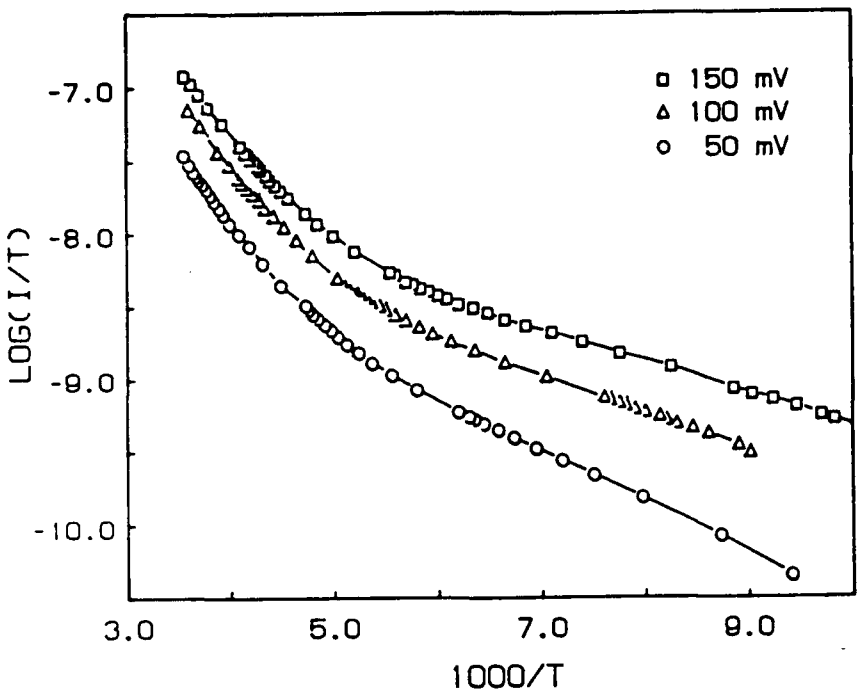

Figure 4: Arrhenius plots for three different biases due to the thermionic emission current through minibands.

are 95 meV and 250 meV, respectively. These values are in good agreement with the calculated values of 91 meV and 220 meV from the emitter band edge taking the heavy and light-hole band splitting into consideration.

3.3 Resonant tunneling transistor

There is a growing interest in the application of resonant tunneling transistors due to expected high speeds into THz frequencies. We have investigated such a transistor using holes in the Si/Ge system since most of the band offset appears at the valence band [5, 6]. The cross-section of the device is shown in Fig. 5(a) consisting of resonant tunneling emitter and a collector. Between the double barrier quantum well emitter and the collector barrier, a base is inserted. Fig. 5(b) shows schematically the band diagram under an external bias. When the emitter is biased positively with respect to the base, holes are injected into the base through the double barrier resonant tunneling emitter with an excess hole energy relative to the valence band maximum of base. The holes injected into the base are then transferred near-ballistically to the collector. The collector barrier prevents injection of the holes initiated from the valence-band of the base to the collector when V_{BC} is applied, while allowing the injected hot holes from the emitter to go through to the collector if these hot holes

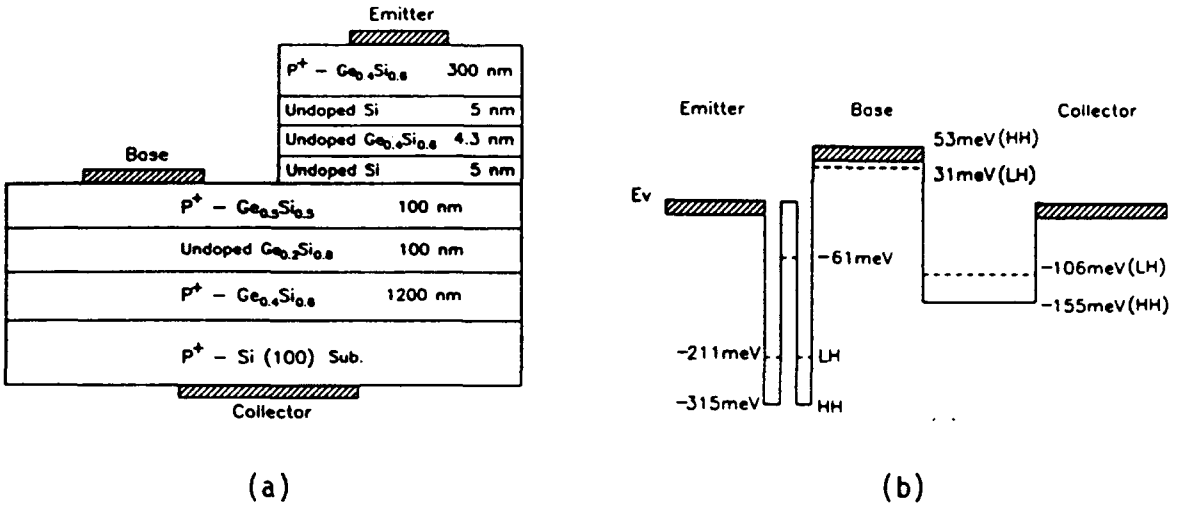

Figure 5: (a) Schematic diagram of a SiGe resonant tunneling hot hole transistor. (b) Valence band diagram of the transistor under an external bias showing the conductance process.

have higher energies than the collector barrier height. The injected holes may suffer some elastic and inelastic scatterings in the base. In the p-doped unipolar structure, the elastic scattering rate is low because the heavy holes are effective in screening static impurities and at low temperature, inelastic scattering may be discounted due to the absence of phonon scattering. Due to the degenerate light and heavy hole bands in the collector, the majority of the current from the collector to the base is due to the light hole because of the lower light-hole barrier height. On the other hand, a larger portion of the base to the collector current at low temperatures may be due to the heavy hole. This is resulted from the lift of degeneracy in the base region where the heavy-hole band is heavily populated at low temperatures.

The common base mode I-V characteristics of the device at 77 K is shown in Fig. 6(a), which gives the collector current I_C as a function of collector voltage V_{BC} for several values of I_E beginning from 0 to 7 mA with a step of 1 mA. Since the barrier height of the collector barrier is only 137 meV for the light hole, the thermionic current is dominant at room temperature. At lower temperatures, the thermionic current decreases while the tunneling current becomes more important. Thus without

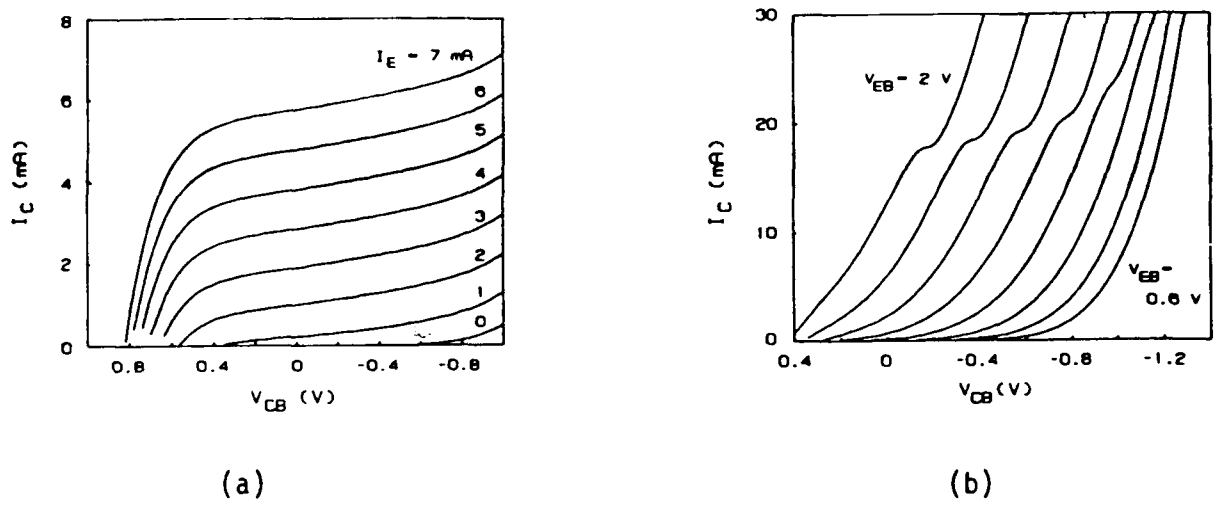

Figure 6: (a) Collector current I_C of the device as a function of V_{BC} at 77 K in a common base configuration. I_E is the parameter for the different curves with a step of 1 mA. (b) Collector current I_C of the device as a function of V_{BC} at 77 K in a common base configuration. V_{EB} is the parameter with a step of 200 mV.

injection from the emitter, I_C consists of thermionic and tunneling current components going over and through the triangular barrier formed by V_{BC} and with perhaps some leakage current due to recombination via defects present in the strained films. In Fig. 6(b), a set of collector currents (I_C) is shown as a function of the base-collector voltage (V_{BC}) at 77 K, with V_{EB} as a parameter. The rightmost curve corresponds to V_{EB} = 600 mV and others are for an incremental step of 200 mV. At V_{EB} = 600 mV, no NDR is observed since a large portion of the collector current comes from the becomes apparent, and the NDR ratio increases with V_{EB}.

3.4 Summary

In summary, there are significant results from the ONR supported research. Among these are, demonstrated resonant tunneling diodes and transistors of the holes and the understanding of the interference of the light and heavy hole tunneling channels. The miniband transport in SiGe/Si superlattices has been demonstrated and the position of the minibands are obtained using thermionic emission analysis. A hot hole transistor has been demonstrated with controllable negative resistance.

References

[1] K. L. Wang, R. P. Karunasiri, J. Park, S. S. Rhee, and C. H. Chern. *Superlattices and Microstructures*, 5(2), 201, 1989.

[2] K. L. Wang and C. H. Chern. Resonant tunneling of holes in strain layer structures. Proc. Workshop on Resonant Tunneling Physics and Applications, El Escorial, Spain May 14-18, (1990).

[3] Ulf Gennser, V. P. Kesan, S. S. Iyer, T. J. Bucelot, and E. S. Yang. *J. Vac. Sci. Technol. B*, 8(2), 210, 1990.

[4] J. S. Park, R. P. G. Karunasiri, K. L. Wang, C. H. Chern, and S. S. Rhee. *Appl. Phys. Lett.*, 54, 1564, 1989.

[5] S. S. Rhee, G. K. Chang, T. K. Carns, and K. L. Wang. *Appl. Phys. Lett*, 56(11), 1061, 1990.

[6] G. K. Chang, T. K. Carns, S. S. Rhee, and K. L. Wang. *to be published*, 1990.

4 Publications Resulted from the ONR Supported Research

J. S. Park, R. P. G. Karunasiri, and K. L. Wang, "Study of Hole Transport Through Minibands in Symmetrically Strained Ge_xSi_{1-x}/Si Superlattice", Thin Solid Films, 183, 25 (1989).

J. S. Park, R. P. G. Karunasiri, and K. L. Wang, "Observation of Large Stark Shift in Ge_xSi_{1-x}/Si Multiple Quantum Wells", J. Vac. Sci. Tech., B8, 217 (1990).

Karunasiri, R. P. G., Park, J. S., Wang, K. L., and Chen, L- J., "Intersubband Infrared Absorption Ge_xSi_{1-x}/Si Superlattice by Photocurrent Measurement", Appl. Phys. Lett., 56, 1342 (1990).

Rhee, S. S., Chang, G. K., Carns, T. K., and Wang, K. L., "SiGe Resonant Tunneling Hot Hole Carrier Transistor", Appl. Phys. Lett., 56, 1061 (1990).

CONTRIBUTIONS TO SEMINARS AND CONFERENCES:

K. L. Wang, "MBE Growth and Properties of SiGe Heterostructures", SRC-TRC, MIT, Boston, September 25-26, (1989).

K. L. Wang, "Growth and Device Application of SiGe Heterostructures", International Conference on VLSI and CAD, Seoul, Korea, October 17-20, (1989).

Rhee, S. S., Chang, G. K., Carns, T. K., and Wang, K. L., "SiGe Resonant Tunneling Hot Carrier Transistor", Proceedings IEEE/IEDM, 27.4.1, 651-654, (1989).

Thin Solid Films, *183* (1989) 25–31

STUDY OF HOLE TRANSPORT THROUGH MINIBANDS IN SYMMETRICALLY STRAINED Ge_xSi_{1-x}/Si SUPERLATTICES

J. S. PARK, R. P. G. KARUNASIRI AND K. L. WANG

Device Research Laboratory, 7619 Boelter Hall, Department of Electrical Engineering, University of California, Los Angeles, CA 90024 (U.S.A.)

(Received May 30, 1989)

The hole transport through the minibands of symmetrically strained Ge_xSi_{1-x}/Si superlattices is observed. The superlattices are grown on unstrained $Ge_{x/2}Si_{1-x/2}$/Si buffer layers. Two peaks are observed from the current–voltage (I–V) and conductance–voltage (dI/dV) measurements, which are due to conduction of light holes through minibands in the superlattice. The second peak shows a negative differential resistance (NDR) region below 100 K. The energies of the minibands are estimated by thermionic emission analysis of current–voltage–temperature (I–V–T) data. Also, we have studied the long wavelength (10 μm) infrared absorption of these superlattice samples by photocurrent measurement. The measured photocurrent as a function of bias shows characteristics similar to the I–V charactetistics. The preliminary data on polarization dependence of the photocurrent suggest that the infrared absorption occurs between light hole minibands.

1. INTRODUCTION

The strained layer Ge_xSi_{1-x}/Si heterostructures and superlattices have created a great deal of interest because of the potential of integration with the conventional silicon very large scale integrated technology. With the current advances in silicon molecular beam epitaxy (Si-MBE), device quality Ge_xSi_{1-x} layers with controlled strain have become possible. Recently, resonant tunneling of holes through double barrier diodes has been reported in variously strained Si/Ge_xSi_{1-x}/Si heterostructures[1–3]. The successful demonstrations of resonant tunneling in the GeSi/Si heterostructures indicate that the GeSi/Si interfaces are of high quality for the fabrication of quantum devices. They further suggest the possibility of superlattice devices using GeSi/Si. In this paper, we report the study of hole miniband transport and intersubband infrared absorption in the short period Ge_xSi_{1-x}/Si superlattices grown on $Ge_{x/2}Si_{1-x/2}$ buffer layers.

2. EXPERIMENTAL DETAILS

The samples used in the experiments are grown in an Si-MBE system with a

0040-6090/89/$3.50

base pressure of approximately 7×10^{-11} Torr. The growth temperature and pressure are 530 °C and 6×10^{-9} Torr respectively. P-type doping is obtained using a thermal boron source[4].

A typical structure is grown on a p^+-doped Si(100) wafer, and it consists of a p-doped $Ge_{0.4}Si_{0.6}$/Si superlattice (15 periods 50 Å thick for each layer) grown on an unstrained p^+ $Ge_{0.2}Si_{0.8}$ buffer layer doped to 5×10^{18} cm^{-3}. A 7000-Å-thick p^+ $Ge_{0.2}Si_{0.8}$ cap layer is grown for ohmic contacts. The $Ge_{0.2}Si_{0.8}$ buffer and cap layers are unstrained, and the $Ge_{0.4}Si_{0.6}$/Si layers in the superlattice are symmetrically strained. This strain symmetrization of the superlattice allows the growth of as many periods as desired without suffering the critical thickness limitation[5]. The samples for the infrared measurement are similar to the above except that they are grown on a p^- substrate (100 Ω cm) for reducing the free carrier absorption. Mesa diodes, 50–100 μm in diameter, are fabricated for electrical and optical measurements.

The current–voltage ($I-V$), and conductance–voltage (dI/dV–V) are measured using a tunneling spectroscopy set-up at different temperatures. Photocurrent of the samples at or near 10 μm is measured at 77 K using a lock-in amplifier and a tunable CO_2 laser.

3. RESULTS AND DISCUSSION

3.1. *I–V and dI/dV Measurements*

Figure 1 shows the measured $I-V$, and dI/dV for the superlattice sample at 4.2, 35 and 77 K. Two peaks at 1.1 and 2.5 V (77 K) are present in the $I-V$ and dI/dV. The peak at 2.5 V shows a clear negative differential resistance (NDR). As the temperature of the sample is decreased, the peak-to-valley ratio of the peak at 2.5 V increases, and the peak at 1.1 V becomes more apparent from the dI/dV curve.

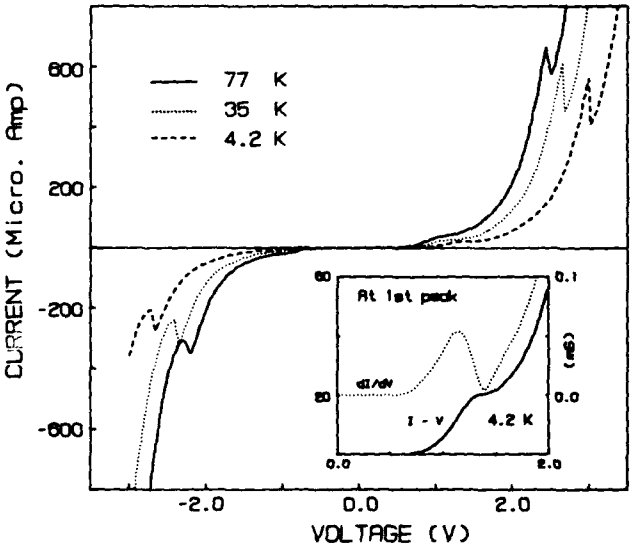

Fig. 1. Observed current–voltage ($I-V$) at 77, 35 and 4.2 K, showing conduction through minibands in the superlattice. Inset of the figure shows the magnified $I-V$, and dI/dV for the first peak.

In order to understand the data, it is necessary to consider the band structure of the sample. The schematic band diagram of the sample is shown in Fig. 2. The barrier heights for the light and the heavy holes, measured from the respective band edges, are 215 and 302 meV. These band offset values are obtained based on the data given in refs. 6 and 7. The strain in $Ge_{0.4}Si_{0.6}/Si$ causes the splitting of the light and heavy hole bands in the superlattice.

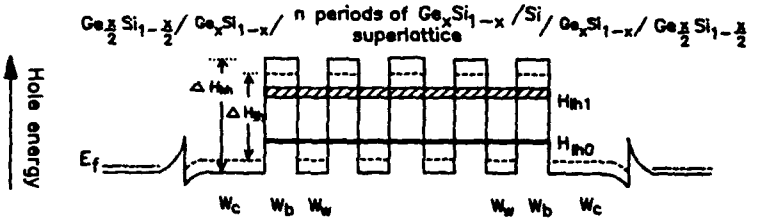

Fig. 2. Schematic band diagrams of the structure used in the present experiment. The device parameters are $n = 15$, $x = 0.4$, $W_c = 150$ Å, $W_b = 50$ Å, $W_w = 50$ Å, ΔH_{hh} (heavy hole barrier height) = 302 meV, ΔH_{lh} (light hole barrier height) = 215 meV, and heavy hole and light hole band splitting equals 39 meV.

The energies and widths of the hole minibands are estimated using the Krönig–Penny model[8] in the effective mass framework. The effective masses of the light and heavy holes in Ge_xSi_{1-x} are deduced from the linear interpolation of bulk silicon and germanium effective masses. Two light hole minibands at 52 (LH_0) and 181 (LH_1) meV from the light hole band edge are found. For the heavy holes, only localized bound states are obtained owing to the relatively high barrier as well as the larger effective mass.

Most of the carriers injected from the emitter travel through the undoped contact layer without scattering, and incident upon the superlattice barrier. The conduction through minibands occurs when the Fermi level in the emitter region is aligned with the bottom of a miniband. The NDR shows up when the Fermi level is moved away from the minibands. The dI/dV data show a rather broad first peak. Since the ideal bandwidth of the first miniband is small, the transport through it may involve phonon-assisted processes (hopping) rather than simple miniband conduction. The heavy hole transmission coefficient is smaller than that of the light hole owing to its larger effective mass and higher potential barrier. Therefore the heavy hole current through the superlattice is negligible compared with the light hole current.

3.2. I–V–T Measurement

In order to obtain the energies of the minibands, we have carried out the I–V–T measurement. At low bias, thermionic emission through miniband energies of the superlattice is the predominant component in carrier transport. The thermionic emission current through a miniband of bandwidth ΔH (when $\Delta H < kT$) in a superlattice is given by the following equation[9],

$$J = \frac{A^* T(E) \Delta H}{k} T \exp\left(\frac{-\phi(V)}{kT}\right) \tag{1}$$

where A^* is the effective Richardson constant, T is the temperature, k is the Boltzmann constant, $\phi(V)$ is the potential difference between the bottom of the miniband and the emitter Fermi level, V is the bias voltage, and $T(E)$ is the tunneling transmission coefficient.

Figure 3 shows the measured I–V–T data of the superlattice sample. For a given bias, two regions with different slopes are observed. One appears in a relatively high temperature region (200–300 K), while the other appears in a lower temperature region (100–170 K). This observation indicates that there are two different thermionic current components (through the first and the second minibands) flowing in the superlattice, as expected. In the low temperature region, most of the thermionic current is from the first miniband at the lower energy, whereas in the higher temperature region, the increased thermal energy allows the carriers to flow through the second miniband as well. The latter component of current is dominant because of the larger bandwidth of the second miniband. Assuming the thermionic current due to the second miniband is negligible at low temperature, one can estimate $\phi_0(0)$ of the first miniband from the experimentally obtained slopes. Figure 4(a) shows the plots of $\lg(I/T)$ *vs.* $1/T$ at several biases. The slope of each plot is obtained by least-squares fitting the data points. Figure 4(b) shows the plots of $\lg(I/T)$ *vs.* $1/T$ corresponding to the high temperature region. In order to obtain the activation energy for the second miniband ($\phi_1(0)$), we have subtracted the current contribution of the first miniband by extrapolating the low temperature data of the current to the high temperature region.

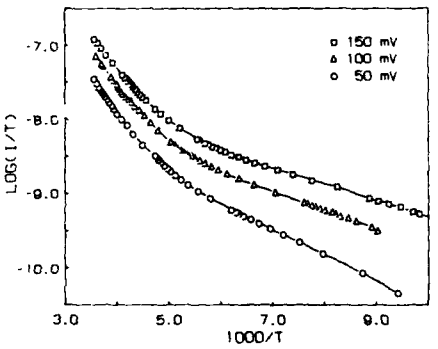

Fig. 3. Arrhenius plots for three different biases due to the thermionic emission current through minibands.

By extrapolating, $\phi(V)$s obtained from Figs. 4(a) and 4(b), $\phi_0(0)$ and $\phi_1(0)$ can be found. The experimentally obtained values for the first and second minibands are 95 meV and 250 meV respectively. These values are in good agreement with the calculated values of 91 and 220 meV from the emitter band edge including heavy and light hole band splitting. Here, we have assumed a Fermi level at the degenerate valence band, and ignored the band bending at the barrier interface and in the barrier.

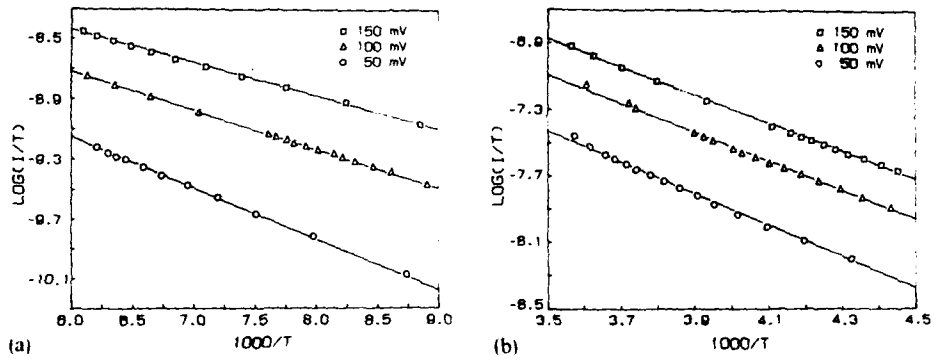

Fig. 4. Plots of $\lg(I/T)$ vs. $1/T$ (a) in the low temperature region (100–170 K) and (b) in the higher temperature region (200–300 K).

3.3. *Photocurrent Measurement*

We have studied the infrared absorption of the superlattice samples by photocurrent measurement using a tunable CO_2 laser. The structure of this sample is the same as the previous samples, except that 60-Å-thick wells and 40-Å-thick barriers are used to obtain a light hole miniband separation near 10 μm. Ohmic contacts are made on the top of cap layer and $Ge_{0.2}Si_{0.8}$ buffer layer. The $I-V$ and dI/dV data (not given) show characteristics similar to the samples grown on a p^+ substrate. However, the current peak positions are observed at higher voltages (1.5 and 5.0 V). This may be due to a higher contact resistance at the buffer layer.

In order to measure the intersubband absorption between the minibands, a 45° angle is polished on the substrate as shown in the inset of Fig. 5. This enhances the electrical field of the light normal to the superlattice plane. Less than 100 μW of CO_2 laser power is incident on the active device area. With the CO_2 laser wavelength fixed at 10.6 μm, the photocurrent signal at 77 K is measured as a function of bias (across a 1 kΩ load resistor).

Curve (a) of Fig. 5 shows the measured photocurrent *vs.* bias, with Z-polarized light (polarization of infrared normal to the plane of the superlattice). It clearly shows two negative differential photoconductivity regions close to the voltages where the peaks in the $I-V$ and dI/dV data are found. To observe the polarization dependence of the infrared absorption, the photocurrent is measured with XY-polarized infrared (polarization of infrared parallel to the superlattice plane). In this case the intersubband transition is forbidden from the selection rule[10]. Curve (b) of Fig. 5 shows the bias dependence of photocurrent for the XY-polarized case, showing almost no bias dependence. No clear peaks are observed, and the photosignal is smaller than that for the Z-polarized case. This results in good agreement with the selection rule.

The data of Fig. 5 can be explained by considering the valence band structure of the sample including the split-off band. At thermal equilibrium, the hole population in the minibands is small. However, under bias, the hole density in the minibands increases by hole injection from the contact. The maximum population is attained when the emitter Fermi level is aligned with a miniband. Under these resonant

conditions, strong infrared absorption can be expected owing to the high density of carriers in the miniband. This accounts for the enhancement of the photocurrent at peak positions of the $I(V)$ curve. The strong polarization dependence of photocurrent suggests that the observed transitions are due to intersubband absorption of infrared. The close agreement of the photocurrent peak positions with the estimated light hole miniband positions suggests that Z-polarized transitions are probably due to $LH_0 \rightarrow LH_1$ and $LH_1 \rightarrow LH_2$ (unconfined state). The small photosignal with the XY-polarized infrared may be due to absorption between light and split-off hole minibands. In the latter case, the oscillatory strength are small compared with the intersubband transitions[11].

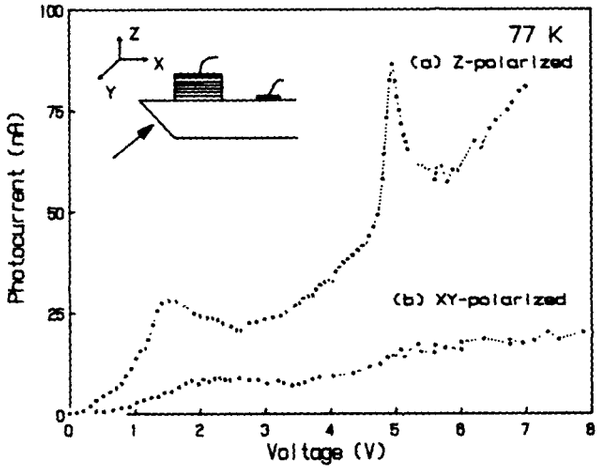

Fig. 5. Photocurrent as a function of bias. A CO_2 laser with wavelength at 10.6 μm is used as a source. (a) With polarization of infrared normal to the superlattice plane (Z direction), (b) parallel to the superlattice plane (XY direction). Inset shows light incident on the 45 polished substrate which was used in the experiment.

Further studies including wavelength dependence of the photocurrent should provide more information about the infrared absorption in GeSi/Si superlattices.

4. SUMMARY

In summary, we studied the hole miniband transport in the symmetrically strained, GeSi/Si superlattices. The $I-V$ and dI/dV data showed peaks which are due to the hole transport through the two light hole minibands. The $I-V-T$ measurement was measured to estimate the energies of the minibands. Infrared absorption of the superlattice as a function of bias was studied by photocurrent measurements. The polarization and bias dependences of the infrared absorption suggest that the infrared absorption is due to the transitions between light hole minibands. The results from the experiment suggest the use of GeSi/Si superlattices for electrical and infrared device applications, such as hot carrier and band-aligned superlattice (BAS) devices[12].

ACKNOWLEDGMENTS

This work is in part supported by the Semiconductor Research Corporation, the Army Research Office, and the Office of Naval Research.

REFERENCES

1 H. C. Liu, D. Landheer, M. Buchanan and D. C. Houghton, *Appl. Phys. Lett.*, *52* (1988) 1809.
2 S. S. Rhee, J. S. Park, R. P. G. Karunasiri, Q. Ye and K. L. Wang, *Appl. Phys. Lett.*, *53* (1988) 204.
3 K. L. Wang, R. P. G. Karunasiri, J. S. Park, S. S. Rhee and C. H. Chern, *Superlattices Microstructures*, *5* (2) (1989) 201.
4 S. S. Rhee, R. P. G. Karunasiri, C. H. Chern, J. S. Park and K. L. Wang, to appear in *J. Vac. Sci. Technol. B*, *7* (1989) 327.
5 E. Kasper, H. J. Herzog, H. Jorke and G. Abstreiter, *Superlattices Microstructures*, *3* (2) (1987) 141.
6 C. G. Van de Wall and R. M. Martin, *J. Vac. Sci. Technol. B*, *3* (1985) 1256.
7 R. People, *Phys. Rev. B*, *34* (1986) 2508.
8 P. F. Yuh and K. L. Wang, *Phys. Rev. B*, *38* (1989) 495.
9 J. S. Park, R. P. G. Karunasiri, K. L. Wang, S. S. Rhee and C. H. Chern, *Appl. Phys. Lett.*, *54* (1989) 1564.
10 L. C. West and S. J. Eglash, *Appl. Phys. Lett.*, *46* (1985) 1156.
11 P. F. Yuh and K. L. Wang, to be published.
12 K. L. Wang and P. F. Yuh, *IEEE J. Quantum Electron*, *QE-25* (1989) 12.

Observation of large Stark shift in Ge_xSi_{1-x}/Si multiple quantum wells

J. S. Park, R. P. G. Karunasiri, and K. L. Wang
Device Research Laboratory, Electrical Engineering Department, University of California, Los Angeles, California 90024

(Received 13 September 1989; accepted 9 December 1989)

Large quantum-confined Stark shift is observed in a type II GeSi/Si multiple quantum well structure for the first time. In this experiment, we have employed the photocurrent measurement using reverse biased *p-i-n* diodes with multiple quantum wells in the *i*-region. The photocurrent as a function of bias is carried out at 77 and 300 K. The results show large red shift of the absorption edge which is about 0.75 meV kV^{-1} cm. This suggests the application of GeSi/Si type II structure for nonlinear electro-optics devices near the 1.3 μm range.

I. INTRODUCTION

With the current advances in silicon molecular-beam epitaxy (MBE) technology, GeSi/Si quantum well and superlattice structures have been fabricated, and their transport and optical properties have been studied. For example, *p-i-n* and avalanche photodiodes operating near 1.3 μm,[1,2] hole double-barrier resonant tunneling diodes,[3,4,5] hot hole resonant tunneling transistor,[6] superlattice hole–miniband transport,[7] and superlattice hole intersubband optical transitions[8] have been demonstrated.

It is known that Ge_xSi_{1-x}/Si heterostructures grown on a Ge_ySi_{1-y} buffer layer have a type II band (staggered) alignment where the quantum wells of electrons and holes are formed in different layers.[9] Due to the spatial separation of wave functions in the valence band (VB) and conduction band (CB), the structures with a type II band alignment are expected to have optical properties different from those of type I structures where both the CB and VB quantum wells are formed in the same layer. In type II multiple quantum well (MQW) structures, interband optical transition occurs due to a small overlapping at the tails of CB and VB bound state wave functions adjacent to the heterointerface.[10] This results in a weaker oscillator strength than the type I case, but it can have a large transition energy shift under an electric field, known as quantum-confined Stark effect.[11] The large transition energy shift in type II structures can be utilized for application in electro-optic devices, such as optical modulators and optical switches.[12,13] The optical properties of type II GeSi/Si superlattices are relatively unknown even though type I GeSi/Si heterostructures (i.e., a superlattice grown on a Si buffer layer) have been studied.[1,2,14] In this paper, we report the observation of a large transition energy shift in the GeSi/Si type II multiple quantum well (MQW) structure for the first time. The photocurrent measurement has been employed in this experiment.

II. EXPERIMENTAL

For the experiment, *p-i-n* diodes are fabricated in which the *i* region consists of type II GeSi/Si multiple quantum wells. The samples are grown in a silicon MBE system with a base pressure of about 7×10^{-11} Torr. The growth pressure and temperature are 5×10^{-9} Torr and 530 °C, respectively. The detail of the Si–MBE system and growth procedure is described elsewhere.[3] The *p-i-n* diode structure consists of a *p*-doped (1×10^{18}/cm^3) $Ge_{0.2}Si_{0.8}$ unstrained buffer layer grown on a *p*-type Si (100) substrate, 50 undoped $Ge_{0.4}Si_{0.6}$/Si quantum wells and barriers (70 Å each), and a 0.8 μm *n*-doped (5×10^{16}/cm^3) $Ge_{0.2}Si_{0.8}$ cap layer terminated with a n^+ doped region for Ohmic contacts. The Ge content and superlattice periodicity in the sample are checked by x-ray diffraction. Thermal boron (B) and antimony (Sb) sources are used for *p*- and *n*-type doping, respectively. Mesa diodes of 450 μm in diameter are fabricated by a conventional liftoff and mesa etching technique. Aluminum (Al) ohmic contacts are made on the etched p^+ GeSi buffer layer and n^+ cap layer. To allow larger amount of light to go into the MQW region, a small Al contact (100 μm in diameter) is made on n^+ cap layer. The current–voltage (I–V) characteristics of these diodes show a very good rectifying behavior with a reverse bias breakdown of about 25 V at 77 K.

The photocurrent measurement as a function of bias is carried out at 77 K, and 300 K in the wavelength range of 1–2 μm. Monochromatic light is obtained using a tungsten lamp and a grating. The photoresponse is measured across a load resistor using a lock-in amplifier operating at 500 Hz. To avoid the higher order effects from the grating in the 1–2 μm range, a silicon filter is used. The measured signal is normalized to the incident light intensity using a calibrated PbS detector.

III. RESULTS AND DISCUSSION

Before presenting the measured data, it is necessary to consider the band structure of the sample in order to help understanding of the results obtained from the photocurrent measurement. Figure 1(a) shows the schematic band diagram of the structure at the flat band condition (without considering the built-in potential in the depletion region). The band gaps and band offsets for the valence and conduction bands can be estimated from the calculations of People[15] and Van de Wall and Martin.[16] Figure 1 shows the type II band alignment in the MQW where the hole and electron quantum wells are formed in the $Ge_{0.4}Si_{0.6}$ and Si layers, respectively. In this structure, the $Ge_{0.2}Si_{0.8}$ buffer layer is unstrained while the Si and $Ge_{0.4}Si_{0.6}$ layers in the active

 0734-211X/90/020217-04$01.00

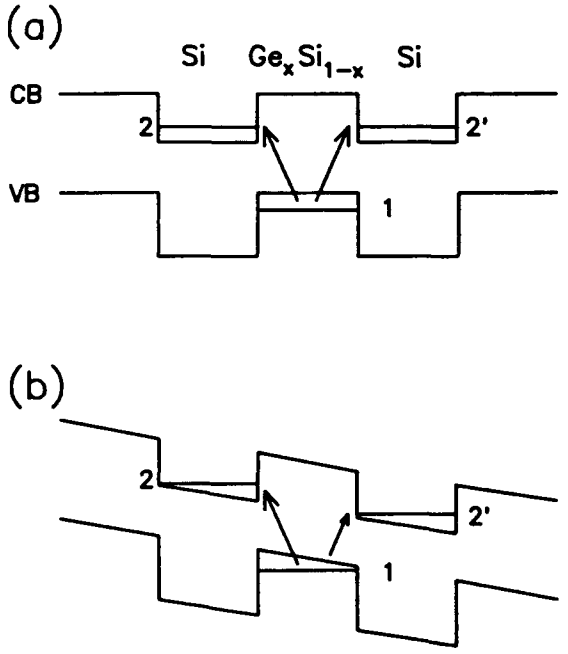

FIG. 1. (a) Schematic band structure of type II Ge_xSi_{1-x}/Si multiple quantum well structure at flat band condition, and (b) under an electric field.

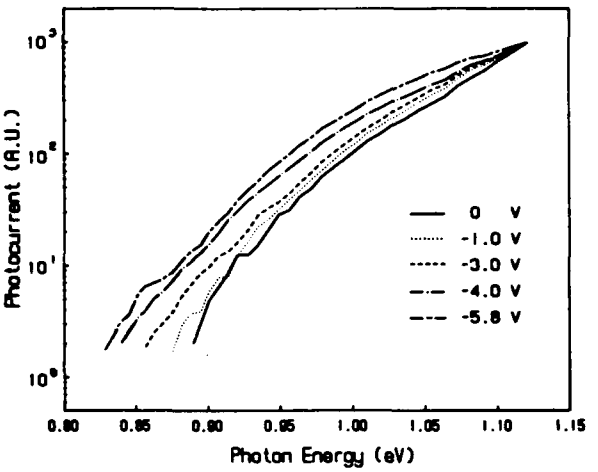

FIG. 2. Normalized photocurrent spectra vs photon energy (77 K) as a function of reverse bias across the *p-i-n* diode.

regions are oppositely strained but with the same magnitude. Thus, the net strain in the structure becomes zero. This strain symmetrization in the structure is useful for optical device application, because thick MQW active layers can be grown to enhance optical absorption without suffering from the critical thickness limitation.

The photocurrent data show strong bias dependent characteristics. Generally speaking, the photocurrent increases as the reverse bias is increased. That is mainly due to the increase of carrier transport under bias in the structure. In order to obtain the spectral data at several biases only corresponding to absorption but to be independent of carrier transport, the obtained photocurrent spectrum at each bias is normalized by the values of 1100 meV. Figure 2 shows the normalized photocurrent versus photon energy as a function of applied reverse bias at 77 K. Similar characteristics are also obtained at 300 K. As can be seen from Fig. 2, the spectra shapes near absorption edge changes as a function of external bias, and this change is attributed to the shift of the transition energy to be discussed next. For an example, the spectral response at 1.3 μm (954 meV) at zero bias at 3% of the response at 1100 meV, but it increases to 10% at 5.8 V. Furthermore, the absorption edges shift to lower energies (red shift) as the reverse bias across the *p-i-n* structure is increased.

This field dependence may be explained in reference to the band diagram shown in Fig. 1. In this structure (type II), since the interband transitions take place due to the overlap of the wave function tails near the heterointerfaces (not at the centers of the wells as in type I case), two different transitions are possible for a VB bound state. One is the transition to the CB states located at the right side of the VB state; and the other at the left side as indicated in Fig. 1(a). At the flat band condition, these transitions have the same energies [$1\rightarrow2$, $1\rightarrow2'$ transitions in Fig. 1(a)]. In the presence of an electric field [Fig. 1(b)], the bands become tilted, and the transition energies shift accordingly. The transitions to the CB states in the neighboring wells, under this condition, are no longer the same. One ($1\rightarrow2'$) shows lowering of the transition energy (red shift), and the other ($1\rightarrow2$) shows rising of the energy (blue shift). The amount of shift is qualitatively given by the potential drop between spatially separated quantum wells (i.e., $eEL/2$, where L is the period of MQW's). As the electric field is increased, both larger red and blue shifts are expected.

The shift of the absorption edges with the applied electric field in Fig. 2 is mainly due to the $1\rightarrow2'$ (heavy hole to conduction band) transitioin. The $1\rightarrow2$ transition is also possible; however, the contribution is appreciable only near the high energy end of the spectrum. This is due to the fact that $1\rightarrow2$ transition energy is considerably higher than $1\rightarrow2'$ transition energy as a result of a larger separation of the energy gap.

In order to determine quantitatively the absorption edge shift, a curve-fitting technique is employed.[14] Each photocurrent spectrum is fitted by the sum of several curves which are expressed in the form of $\alpha(h\nu - E_g)^2$. Figure 3 shows a typical example of a curve-fitting procedure (data at 4.0 V). The spectrum can be best fitted by three curves up to 1.1 eV. The low-energy feature in the background of noise may be due to defect-related absorption, and the first curve (1) fitted to this is subtracted from the spectrum in the higher-energy region for determining the transition edges. The second curve (2) is fitted to the low-energy absorption edge and the red shift of the ground heavy hole state is found. The third curve (3) may be attributed to the light hole transition. On the other hand, the absorption in this region could also arise from the blue shifted transition.

From the data, the lowest absorption edge at zero bias is found to be 871 meV. This value is smaller than the bandgap of both strained bulk Si and $Ge_{0.4}Si_{0.6}$ grown on a $Ge_{0.2}Si_{0.8}$ layer, which have the theoretical values of 1070 and 927

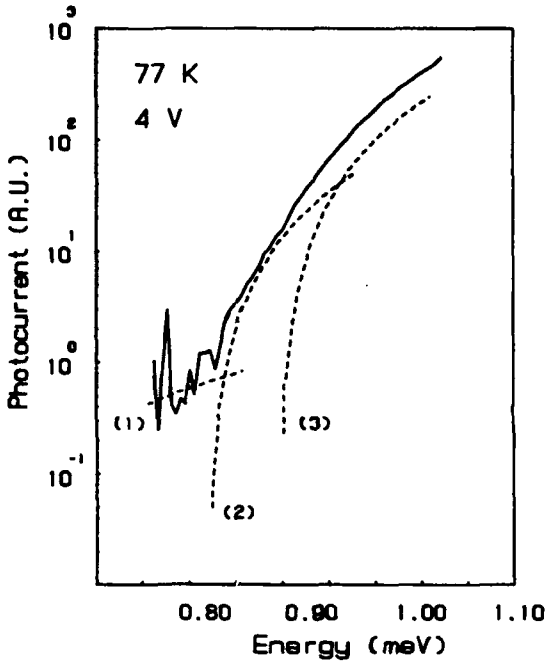

FIG. 3. Typical example of a curve-fitting procedure. The bias across the diode for this spectrum is − 4.0 V.

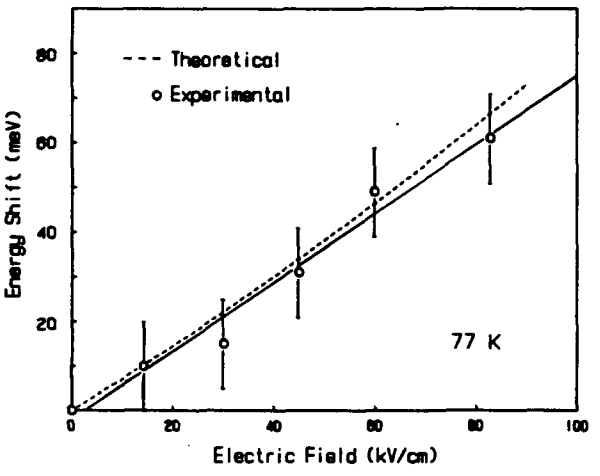

FIG. 4. Electric field vs absorption edge shift (77 K). The data points indicate the experimental values obtained using a curve-fitting technique. The dashed curve shows the theoretical values. Note: zero bias is taken as the reference point.

meV, respectively. This confirms, first of all, that the observed transition occurs in the type II quantum well in our case.

Using the curve-fitting technique, the heavy hole absorption edges at several biases are estimated. The error involved in this technique is about ± 10 meV. The obtained values at each bias are given in Table I. Assuming that most of the applied voltage drops across the undoped multiple quantum well region, the absorption energy shift as a function of electric field can be estimated. These experimental shifts are plotted in the solid curve in Fig. 4. In the plot, the zero biased case is taken as the zero field reference point. The dashed curve shows the calculated absorption energy shift versus electric field in the structure. An envelope function approximation is used for the calculation. The measured shift is approximately 0.75 meV kV^{-1}. The experimentally obtained curve shows good agreement with the calculated curve.

To confirm that the absorption edge shift is due to the nature of the type-II quantum well (not due to carrier transport under an electric field), the obtained results are compared with those of type-I structures. Temkin *et al.* have reported that they observed no spectral shift from the type-I *p-i-n* diodes up to an electric field of 160 kV cm^{-1}.[1] Furthermore, we have also fabricated a type-I *p-i-n* diode which consists of $Ge_{0.6}Si_{0.4}$/Si MQWs in the *i* region. The structure is directly grown on Si (100) substrate. Our results show that the strength of photocurrent depends on the bias. However, when the photocurrent spectra at several biases are normalized as have been done in the type-II case, no appreciable changes in spectral shape are observed, which is in agreement with Temkin's result.

Since the transition in this structure involves an indirect transition in both real and *k* spaces, the theoretrical calculation of absorption spectra as a function of bias is not straightforward. However, the shift of the band edge can be estimated using a simple calculation as discussed before. The results show a large red shift of absorption edges, which is theoretically predicted for a type-II structure.

TABLE I. Estimated heavy hole absorption edges at several biases using the curve fitting technique. The errors involved are about ± 10 meV.

Bias (V)	0	− 1	− 2	− 3	− 4	− 5.8
Energy (meV)	875	865	860	844	826	814

IV. SUMMARY

In summary we have demonstrated the large quantum-confined Stark effect in a type-II GeSi/Si multiple quantum well structure. A *p-i-n* structure with MQW in the *i* region is used, and the photocurrent measurements as a function of bias have been employed for experiment. The photocurrent spectra have shown a large red shift as a function of the applied electric field (0.75 meV kV^{-1} cm). Our experimental results suggest the possible application of type-II GeSi/Si structure for nonlinear electro-optic devices, such as optical modulators and switches.

ACKNOWLEDGMENT

This work is in part supported by the Army Research Office and the Office of Naval Research, and Semiconductor Research Corporation.

[1] H. Temkin, T. P. Pearsall, J. C. Bean, R. A. Logan, and S. Luryi, Appl. Phys. Lett. 48, 963 (1986).
[2] T. P. Pearsall, H. Temkin, J. C. Bean, and S. Luryi, IEEE Electron. Device Lett. EDL-7, 330 (1986).

[3]S. S. Rhee, J. S. Park, R. P. G. Karunasiri, Q. Ye, and K. L. Wang, Appl. Phys. Lett. **53**, 204 (1988).
[4]H. C. Liu, D. Landheer, M. Buchanan, and D. C. Houghton, Appl. Phys. Lett. **52**, 1809 (1988).
[5]K. L. Wang, R. P. G. Karunasiri, J. S. Park, S. S. Rhee, and C. H. Chern, Superlattices and Microstructures **5**, 201 (1989).
[6]S. S. Rhee, G. K. Chang, T. K. Carns, and K. L. Wang, Appl. Phys. Lett. (to be published).
[7]J. S. Park, R. P. G. Karunasiri, K. L. Wang, C. H. Chern, and S. S. Rhee, Appl. Phys. Lett. **53**, 1564 (1989).
[8]R. P. G. Karunasiri, J. S. Park, and K. L. Wang, Appl. Phys. Lett. (to be published).
[9]G. Abstreiter, H. Brugger, and T. Wolf, Phys. Rev. Lett., **54**, 2441 (1985).
[10]B. A. Wilson, IEEE J. Quantum Electronics, **QE-24**, 1763 (1988).
[11]D. A. B. Miller, D. S. Chemla, A. C. Gossard, W. Wiegmann, T. H. Wood, and C. A. Burrus, Phys. Rev. B, **32**, 1043 (1985).
[12]T. H. Wood, C. A. Burrus, D. A. B. Miller, D. S. Chemla, T. C. Damen, A. C. Gossard, and W. Wiegmann, Appl. Phys. Lett. **14**, 16 (1984).
[13]D. A. B. Miller, J. S. Weiner, and D. S. Chemla, IEEE J. Quantum Electron. **QE-22**, 1816 (1986).
[14]D. V. Lang, R. People, J. C. Bean, and A. M. Sergent, Appl. Phys. Lett. **47**, 1333 (1985).
[15]R. People, Phys. Rev. B **34**, 2508 (1986).
[16]C. G. Van de Walle and R. Martin, J. Vac. Sci. Technol. B **3**, 1257 (1985).

Properties and Devices of SiGe Heterostructures and Superlattices

K. L. Wang

Device Research Laboratory
7619 Boelter Hall
Department of Electrical Engineering
University of California
Los Angeles, CA 90024

ABSTRACT

Recent progress in the growth of pseudomorphic SiGe strained layers makes it possible the realization of many advanced heterojunction devices. In this paper, several successful techniques for growth of pseudomorphic strained Ge_xSi_{1-x} layers on Si will be briefly reviewed. The bandgap and the splitting of the bands when subjected to strain will be described. Other strained layer properties such as critical thickness and the strain engineering will be discussed.

Device application based on the success of the material research will also be discribed. The most apparent device in applications to VLSI is heterojunction bipolar transistors (HBT). Other advances including the demonstration of tunneling structures, quantum well structures and new devices based on band aligned superlattices will be presented. Finally, the perspective of possible application of Ge_mSi_n in optoelectronics will be addressed.

1 Introduction

Strained layer Ge_xSi_{1-x}/Si heterostructures and superlattices have created a great deal of interests due to the potential of integration with the conventional silicon VLSI technology. With the current advances in silicon molecular beam epitaxy (Si-MBE) and other low temperature epitaxy techniques, device quality Ge_xSi_{1-x}/Si layers with controlled strain are now available for further advancing the speed performance and the art of Si-based Technology. Several optical and electronic devices, such as Modulation Doped Field Effect Transistors (MODFET) [1, 2], Heterojunction Bipolar Transistors (HBT) [3, 4] and Photo-detectors [5, 6, 7] have been demonstrated with the Ge_xSi_{1-x}/Si system.

The purpose of this paper is to review the current understanding of the fundamental properties of Ge_xSi_{1-x}/Si heterostructures and to assess the present status of the device application efforts. Then a prospective view of the field will follow.

2 Band Structures and Properties Under Strain

The band structure of coeherently strained $Ge_xSi_{1-x}$is affected by the orientation and Ge content of the substrate. The band splitting under strain can be calculated from available deformation potentials. Both measured and calculated values of the valence band offsets are available. However, the conduction band offsets are relatively unknown compared with those of the valence band.

2.1 Conduction Band Splitting of Si and Ge under Strain

According to deformation potential theory [8, 9], the energy shift of the conduction band at valley i for an arbitrary homogeneous deformation can be expressed as:[8]

$$\Delta E_c^i = [\Xi_d 1 + \Xi_u \{a_i a_i\}] : \epsilon \qquad (1)$$

where 1 is the unit tensor, a_i is the unit vector parallel to the $\vec{k}$ vector of the valley i, ϵ is the strain tensor, Ξ_d and Ξ_u are deformation potentials, and { } denotes a dyadic product. The shift of the mean energy of the band extreme is

$$\Delta E_c^0 = (\Xi_d + \Xi_u/3)1 : \epsilon \qquad (2)$$

When Si or Ge is coherently grown on a substrate having a diamond structure with a different lattice constant, the strain tensor is similar to that of biaxial stress case. The quantity $\Delta E_c^i - \Delta E^0$ is given for both Si and Ge for all three growth directions ([001], [111] and [110]) in Refs. [10, 11, 12].

2.2 Valence Band Splitting of Strained Si and Ge

Including the spin-orbit splitting, the valence band of Si and Ge consists of a fourfold $P_{3/2}$ multiplet and a $P_{1/2}$ doublet with a split off band separation of $\Lambda = 0.044$ eV in Si and $\Lambda = 0.29$ eV in Ge. In the coherent growth case,

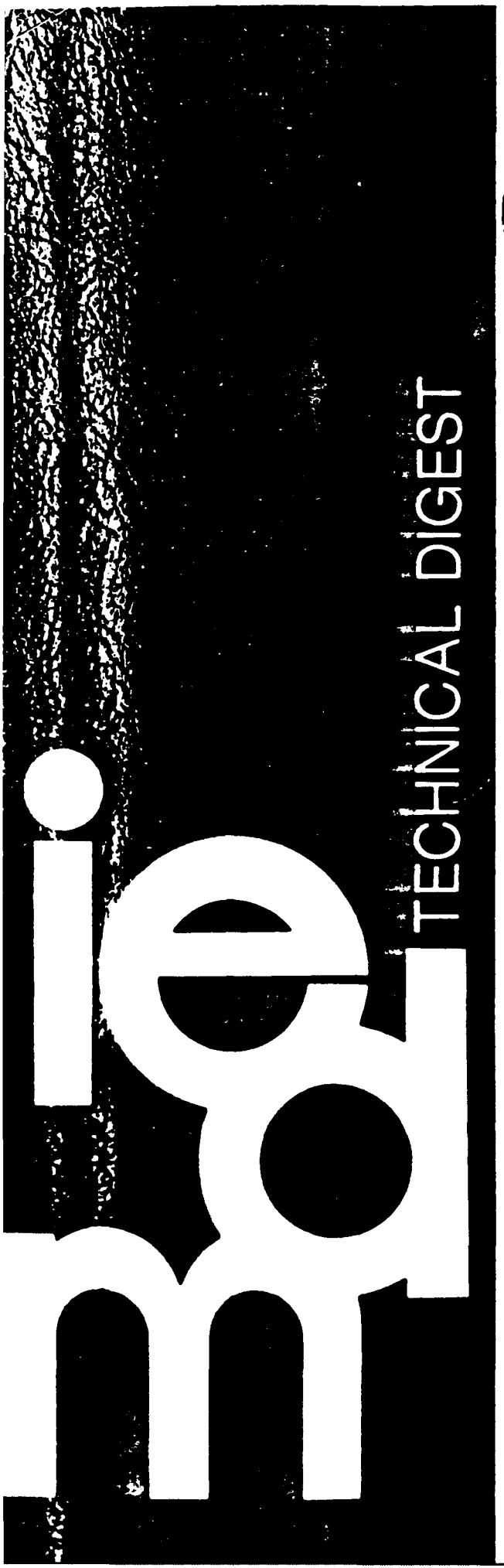

international ELECTRON DEVICES meeting

1989

WASHINGTON, D.C.
DECEMBER 3-6, 1989

Sponsored by Electron Devices Society of IEEE

SiGe RESONANT TUNNELING HOT CARRIER TRANSISTOR

S. S. Rhee, G. K. Chang, T. K. Carns, and K. L. Wang

Device Research Laboratory, 7619 Boelter Hall
Department of Electrical Engineering
University of California, Los Angeles, CA 90024

ABSTRACT

A three-terminal hot hole transistor is fabricated using a Si/GeSi/Si double barrier resonant tunneling structure as an emitter with a thin base in order to obtain near-ballistic transport. The collector current shows a negative differential resistance and strongly depends on the emitter-base voltage. Due to the high speed nature of the tunneling process and negative differential resistance, integration of such device into Si technology could find applications in the areas of high speed digital circuits, frequency multipliers, and tunable oscillators/amplifiers.

Recent developments in Si molecular beam epitaxy (MBE) has made it possible to grow SiGe layers on Si under controlled strain. The device application of such structures focused mainly on the bulk properties of SiGe under strain. However, recent demonstrations of resonant tunneling(1,2) as well as superlattice miniband transport(3) suggest the possible bandgap engineering for other device applications. In SiGe heterostructures, the small light-hole effective mass of SiGe alloys and the band alignments favor hole transport devices(4). In III-V compound heterostructures (mainly in GaAS), several attempts have been made to incorporate the negative differential resistance into three terminal devices by using FET structures(5,6), hot electron transistors(7,8), and bipolar transistor structures(9,10). To the best of our knowledge, three terminal devices incorporating the resonant tunneling feature have not yet been realized in the GeSi heterostructure system. The incorporation of negative differential resistance(NDR) with expected operating frequencies in the THz range(11) into existing advanced Si technology could find potential applications in high speed digital circuits, frequency multipliers, and tunable oscillators/amplifiers. In this letter we report the characteristics of a SiGe hot carrier resonant tunneling transistor.

The samples were grown on highly doped p-type (100) Si substrates in a Si MBE chamber. Detailed procedures for sample cleaning and growth can be found elsewhere(2). Fig. 1 shows the structure of the resonant tunneling transistor. A double barrier structure which consists of two 50 Å Si layers separated by a 43 Å $Ge_{0.4}Si_{0.6}$ quantum well is used as an emitter. A 1.2 μm $Ge_{0.4}Si_{0.6}$ buffer layer acts as a collector and the collector barrier consists of a 1000 Å $Ge_{0.2}Si_{0.8}$ layer. Between the double barrier quantum well emitter and the collector barrier a 1000 Å $Ge_{0.5}Si_{0.5}$ base is inserted. The doping concentration is about $1x10^{18}cm^{-3}$ throughout the device except for the collector barrier and the double barrier resonant tunneling structure, which are undoped. Substrate temperature was held at about 530° C during the growth. The emitter and base contacts were obtained using selective wet etching and standard photolithography techniques. The collector contact was made on the back side of the wafer. Details of the selective etching techniques will be presented elsewhere(12).

The valence-band offsets and bound state energy of the light-hole ground state in the quantum well is shown schematically in Fig. 2. For convenience the hole energy was taken to be positive. All the values are given in reference to the valence-band edge of the unstrained $Ge_{0.4}Si_{0.6}$ layers. The collector barrier and the resonant tunneling double barriers in the emitter are subjected to an in-plane tensile strain which causes the heavy-hole band edge to be above the light-hole band edge. In the base, the heavy-hole band edge is below the light-hole band edge due to the compressive strain. In the unstrained $Ge_{0.4}Si_{0.6}$ layers, the light hole and heavy hole bands are degenerated. The light and heavy holes transporting from the collector to the base have to overcome 106 meV and 155 meV barriers, respectively. On the other hand, the light and heavy holes see the barrier heights of 137 meV and 208 meV, respectively, from the base to the collector. Due to the degenerate light and heavy hole bands in the collector, the majority of the current from the collector to the base is from light holes because of the lower light-hole barrier height. On the other hand, a larger portion of the base to the collector current at low temperatures may be due to heavy holes. This results from the lift of degeneracy in the base region where the heavy-hole band is heavily populated at low temperatures. Thus, the effective barrier height from the collector to the base is 106 meV as seen by the light hole and 208 meV from the base to the collector as seen by the heavy hole. An asymmetric I-V characteristic between the base and the collector was evident as a result of the unequal barrier heights. In the double barrier quantum well emitter, the barrier heights for

CH2637-7/89/0000-0651 $1.00 © 1989 IEEE